Experimental Eye Research 92 (2011) 464–472

Contents lists available at ScienceDirect

Experimental Eye Research

journal homepage: www.elsevier.com/locate/yexer

Optimization of laser-induced choroidal neovascularization in African green monkeys

Robin J. Goody [a], Wenzheng Hu [b], Afshin Shafiee [b], Michael Struharik [a], Stephen Bartels [b], Francisco J. López [b,1], Matthew S. Lawrence [a,*]

[a] RxGen, Inc., 100 Deepwood Drive, Hamden, CT 06517, USA
[b] Preclinical Pharmacology, Bausch & Lomb Inc., Rochester, NY 14603, USA

ARTICLE INFO

Article history:
Received 19 November 2010
Accepted in revised form 6 March 2011
Available online 15 March 2011

Keywords:
laser-induced choroidal neovascularization
age-related macular degeneration
nonhuman primate
African green monkey
Chlorocebus sabaeus
animal model
VEGF

ABSTRACT

We developed and validated a new nonhuman primate model of laser-induced choroidal neovascularization (CNV) that addresses study design limitations prevalent in laser-induced CNV-based efficacy studies. Laser-induced Bruch's membrane disruption triggers CNV and has been widely utilized in animals to model neovascular ("wet") age-related macular degeneration (AMD). Despite widespread use of the approach, detailed assessment of experimental parameters and their influence on pathophysiological endpoints critical for disease modeling has been extremely limited and largely based on anecdotal observations. We evaluated laser power parameters and endpoint measures to optimize methods for CNV formation and quantification to facilitate drug efficacy screening in African green monkeys. Six laser spots of 350, 550, 750, 950 or 1500 mW laser power were positioned bilaterally 1.5 disc diameters from the fovea, within the macula. Fluorescein angiograms were collected 3–5 weeks later and scored by trained masked investigators using graded (I–IV) and densitometric methods. Histopathology assessments were also performed, including determination of CNV area. Test system sensitivity to angiogenesis inhibition was subsequently assessed by evaluating the effect of intravitreal bevacizumab (Avastin) pretreatment (one day prior to laser photocoagulation) on incidence of CNV. Grade III and grade IV lesions were considered clinically relevant, demonstrating early hyperfluorescence and late leakage within or beyond the lesion borders. By 4 weeks post-laser all treatment groups demonstrated evidence of grade III lesions with greatest incidence observed in lesions induced by 750 and 950 mW laser power (72.9% and 69.4% respectively). Grade IV lesions were confined to eyes receiving 550 mW laser power or higher, with highest incidence of grade IV lesions observed in eyes receiving 950 (19.4%) and 1500 mW (31%) laser spots, incidence peaking 4 weeks post-laser photocoagulation. Densitometric analyses of angiograms corroborated visual scoring. Bevacizumab completely abolished grade IV lesion development and significantly lowered lesion fluorescein signal intensity ($P < 0.0001$) and CNV area ($P = 0.038$) compared to vehicle-treated controls. Our studies demonstrate that laser power of 950–1500 mW and angiography analysis 4 weeks post-laser are optimal parameters to evaluate treatment effects on CNV induction following laser photocoagulation. Bevacizumab significantly attenuated CNV development, as determined by fluorescein angiography and histopathology assessments in this model, supporting the application of African green monkeys in preclinical modeling of CNV. Laser parameters and time points for therapeutic dosing and angiography endpoints are critical factors to the laser-induced CNV model and must be validated for robust assessment of efficacy. The newly optimized nonhuman primate model described will facilitate preclinical efficacy assessments of novel therapeutics for CNV.

1. Introduction

Choroidal neovascularization (CNV) involves the invasion of new blood vessels from the choroid through breaks in Bruch's membrane. Choroidal neovascularization is a feature of several eye diseases, but is most commonly associated with age-related macular degeneration (AMD). In the advanced "wet" form of AMD, CNV develops in the choriocapillaries and subretinal space, disrupting the retinal pigment epithelium (RPE) and resulting in severe central vision loss (Green, 1999). Age-related macular degeneration remains a leading cause of blindness in older populations of developed countries (Resnikoff et al., 2004). Recent development of anti-vascular endothelial growth factor

* Corresponding author. Tel.: +1 203 498 9706; fax: +1 203 776 2893.
E-mail address: mlawrence@rx-gen.com (M.S. Lawrence).
[1] Current address: Integrative Pharmacology, Life Sciences, Corning Incorporated, One Science Center Drive, Corning, NY 14831.

0014-4835/$ – see front matter © 2011 Elsevier Ltd. All rights reserved.
doi:10.1016/j.exer.2011.03.006

(anti-VEGF) therapies has dramatically improved outcome for many patients with AMD (Ozkiris, 2010). The anti-VEGF agents pegaptanib sodium (Macugen™, Eyetech, Inc., New York, NY), ranibizumab (Lucentis™, Genentech, Inc., South San Francisco, CA) and bevacizumab (Avastin™, Genentech, Inc.) have all demonstrated efficacy at attenuating vision loss or improving visual acuity in the clinic following repeated intravitreal (IVT) injection (for review, see Ciulla and Rosenfeld, 2009). However, anti-VEGF based therapeutics are not effective in all patients. In the 2006 MARINA trial, substantial vision improvement was confined to only a third of patients; and in 1/6th of trial patients the disease still progressed to legal blindness over a 24 month period (Rosenfeld et al., 2006).

Early clinical observations of CNV 4–6 weeks after argon laser-mediated photocoagulation therapy for macular degeneration provided the basis for the development of animal models of the disease (Francois et al., 1975). Significantly, recent studies evaluating ranibizumab and bevacizumab in rat (Lu and Adelman, 2009) and mouse (Yu et al., 2008) models of CNV demonstrated that these humanized anti-VEGF antibody-based therapeutics offer no improvement in leakage or neovascularization in rodent models. The absence of efficacy in rodent models is presumed to be related to the structural differences between rodent and human VEGF. Due to the unique shared physiology and anatomy of human and nonhuman primate eyes, the primate laser-induced CNV model, which has been investigated in rhesus (Ryan, 1979; Zhang et al., 2008) and cynomolgus monkeys (Tolentino et al., 2000; Shen et al., 2004), has become the model of choice for preclinical evaluation of the efficacy of candidate wet AMD therapies, including the VEGF inhibitors, now in clinical use. This is exemplified by the efficacy of ranibizumab at attenuating CNV alone (Krzystolik et al., 2002) and in combination with verteporforin photodynamic therapy in cynomolgus monkeys (Husain et al., 2005; Kim et al., 2006) and the recent first demonstration of efficacy of bevacizumab in a cynomolgus monkey model (Lichtlen et al., 2010). The relative expense and scarcity of rhesus and cynomolgus monkeys, however, can be a prohibitive barrier in the evaluation of novel therapeutics. In contrast, the African green monkey (*Chlorocebus sabaeus*) is another well-validated old world primate model species (Carlsson et al., 2004) with greater abundance and available for research use at potentially more reasonable cost. Furthermore, use of this species in ophthalmic studies has been reported since the early 1960s (Barany, 1963, 1977; Merrill and Burge, 2007). Early evaluations of laser-induced CNV in nonhuman primates demonstrated low incidence of CNV (Ryan, 1982; Shen et al., 2002), however, more recent studies have shown increased CNV incidence after photocoagulation in the macular region (Shen et al., 2004). Laser photocoagulation has been performed with various laser parameters over recent years. A spot size of 50 μm and duration of 100 ms has been most widely used in nonhuman primates (Ryan, 1982; Shen et al., 2004; Husain et al., 2005). Laser power, however, has been more variable between research groups, ranging from 240 mW (Zhang et al., 2008) up to as high as 1500 mW (Shen et al., 2004). Significantly, while laser power settings of 300–700 mW are most commonly described (Miller et al., 1995; Husain et al., 2005; Koh et al., 2006; Zhang et al., 2008), many groups utilize a multiple hit approach, whereby laser photocoagulation is repeated at either the same spot or an immediately adjacent one until an audible "pop" is heard and a subretinal bubble visualized as Bruch's membrane is disrupted.

The objective of these studies was to validate a laser-induced CNV model of wet AMD in the African green monkey by demonstrating angiographically and histopathologically evident neovascularization following laser injury and by showing inhibition of neovascularization in this model by a well characterized existing therapeutic. This model represents a new nonhuman primate model and an optimal study design for assessment of efficacy of novel wet AMD therapeutic candidates.

2. Materials and methods

2.1. Animals

Twenty-four male African green monkeys (*C. sabaeus*), aged 4–8 years were used in accordance with the ARVO Statement for the Use of Animals in Ophthalmic and Vision Research. Permission allowing the use of bilateral treatments and all aspects of the animal studies was obtained from the primate facility (St. Kitts Biomedical Research Foundation, St. Kitts, West Indies) Animal Care and Use Committee. Monkeys were anesthetized for all procedures with intramuscular injection of 5:1 ketamine:xylazine mix (0.2 mL/kg of 100 mg/mL ketamine and 20 mg/mL xylazine). Supplemental anesthesia (ketamine:xylazine) was administered intramuscularly as needed. Proparacaine hydrochloride 0.5% was provided topically. Animals were euthanized using intravenous pentobarbital sodium and enucleation performed immediately thereafter.

2.2. Induction of experimental CNV

Baseline fundus photography and fluorescein angiograms were performed as part of animal and ocular health screening (day -1) prior to laser photocoagulation. On day 0, monkeys were randomly assigned to treatment groups. Six laser spots were concentrically spaced approximately 1.5 disc diameters from the fovea at the anatomic periphery of the macula, within the temporal vascular arcades. Laser spots were applied using an Iridex Oculight TX 532 nm laser at 350–1500 mW power. Laser pulse duration and spot size were fixed at 100 ms and 50 μm, respectively. A single laser photocoagulation treatment was provided per site, independently of the presence or absence of an audible "pop" sound and visualization of a subretinal bubble, which are routinely used as indications of successful disruption of Bruch's membrane. The laser was mounted on a slit lamp with a slit lamp adapter and the beam directed to the retina with a Volk Centralis Direct ANF+ 0.9× laser lens with a 10 mm contact diameter (Volk Optical, Mentor, OH). Saline was used as the coupling agent. In experiments assessing efficacy of bevacizumab a laser power of 1500 mW was used with all other parameters identical to that detailed here.

2.3. Ocular examinations

Eyes were examined by slit lamp and indirect ophthalmoscope immediately prior to IVT injections on day 0, immediately prior to laser treatment on day 1 and on days 15 and 22.

2.4. Laser power assessment

To determine optimal laser power for development of grade IV CNV lesions in African green monkeys 16 adult males were randomly assigned into treatment groups receiving 350, 550 (3 animals per group), 750 or 950 mW (4 animals per group) laser power. A separate cohort of four adult males received 1500 mW laser power, and was analyzed separately. No additional treatments were performed on these animals prior to or following laser treatment and all other parameters for lesion induction were as described above.

2.5. Bevacizumab treatment

To assess efficacy of an existing wet AMD therapeutic in this model, 8 adult male African green monkeys were randomly

assigned to bevacizumab or vehicle treatment groups (4 animals per treatment group). One day prior to laser treatment (1500 mW laser power, 100 ms pulse duration and 50 μm spot size) animals received bilateral IVT injection of 50 μl bevacizumab (1.25 mg/eye) or vehicle (saline). Animals were euthanized at day 29 post-laser. Lyophilized bevacizumab (Genentech, Inc.) was stored at 2–8 °C. The drug was reconstituted on the day of injection to a concentration of 25 mg/mL using vehicle (0.9% sterile saline) provided by the manufacturer. After animals were anesthetized, a drop of proparacaine hydrochloride 0.5% and then 5% betadine solution was administered to each eye, followed by rinsing off of excess betadine using sterile saline. A self-retaining eye speculum was placed in the eye to facilitate administration. Intravitreal injections of 50 μL of bevacizumab or vehicle were administered per eye using a 30-gauge needle. Four animals received bilateral bevacizumab treatment, the remaining 4 animals received bilateral vehicle. Intravitreal injections were followed by topical administration of 1–2 drops of Vigamox (0.5% moxifloxacin hydrochloride) antibacterial ophthalmic solution (Alcon Laboratories, Inc., Fort Worth, TX).

2.6. Fundus photography

Fundus color photography and angiography was performed on anesthetized animals using a retinal camera (model TRC 50X; Topcon America Corp., Paramus, NJ) with Canon 5D digital imaging hardware and New Vision Fundus Image Analysis System software. Fluorescein angiography in the left eye preceded angiography in the right eye by one day to allow adequate time for wash out of fluorescein between image series. Color and red-free images were collected from each eye prior to infusion of 0.1 mL/kg 10% sodium fluorescein into the saphenous vein. A rapid series of angiogram images were collected from the posterior pole immediately after completion of the infusion for the first minute, and then at approximately 2, 3, 6 and 10 min. A single angiogram was also taken from the contralateral eye after collection of the 10-minute angiogram image to ensure inter-eye consistency in fluorescein levels in the optic nerve head and normal vasculature. Color and red-free photographs and fluorescein angiograms were collected from each animal at 15, 22, 29 and 36 days (left eye) and at 16, 23, 30 and 37 days (right eye) after laser for studies determining optimal laser power and at 21, 28 (left eye), 22 and 29 days (right eye) for efficacy assessments.

2.6.1. Fluorescein angiography scoring

Scoring of angiograms post-laser treatment was performed by examiners masked to treatment using a previously validated methodology (Krzystolik et al., 2002; Husain et al., 2005; Zhang et al., 2008). CNV was rated on a I to IV scale where I = no hyperfluorescence; II = hyperfluorescence without leakage; III = hyperfluorescence early or mid-transit with late leakage; IV = hyperfluorescence early or mid-transit with late leakage extending beyond the borders of the treated area. Lesions were graded systematically from the 12 o'clock position in a clockwise manner. Fluorescein intensity was quantified within lesions in 6 min angiograms using ImageJ (NIH, Bethesda) with a 300 pixel diameter circle positioned over spots to determine mean, background-corrected signal intensity. This densitometry technique is based on previously published methods (Marano et al., 2005; Marano and Rakoczy, 2006; Takahashi et al., 2006; Lichtlen et al., 2010). ImageJ software (National Institute of Health [NIH], Bethesda, MD) was used to analyze signal intensities in each laser spot by an investigator masked to treatment. An identically sized circle was also drawn over an area proximal to the lesion but not containing lesions and avoiding any major veins or arteries or the fovea. This measure provided the background mean gray value for that angiogram image, which was then subtracted from all lesion values to provide background-corrected intensity (relative fluorescence) values. Background correction was performed in this manner on each angiogram analyzed. A constant circle size was used to avoid bias related to poorly defined lesion perimeters in late phase angiograms. Analysis of 3–5 week angiograms using this approach facilitated thorough and reliable analysis of the time course of lesion development and the effect of bevacizumab treatment on leakage.

2.7. Histopathological analysis

Globes were carefully enucleated and anterior segments removed. Posterior poles were fixed overnight in Karnovsky fixative (2% glutaraldehyde, 2.5% formaldehyde in 0.1 M sodium cacodylate buffer) before replacement of fixative with 0.1 M sodium cacodylate buffer. Posterior poles were mounted into tissue blocks and 5 μm serial sections cut at 100 μm intervals and stained with hematoxylin and eosin (HE) by Vet Path Services, Mason, OH.

Flat mounts of retina and choroid/RPE were soaked in PBS containing 0.5% Triton-X overnight at 4 °C before incubating in PBS with 0.25% trypsin solution containing 0.038% EDTA without $CaCl_2$, $MgCl_2$ for 2 h at 37 °C. After cooling for 10 min, tissue was rinsed in two 5 min washes in PBS containing 0.05% TWEEN-20 (PBST). Tissue was blocked for 1 h in 5% normal goat serum before overnight incubation with anti-von Willebrand factor (anti-vWF) antibody (Dako, Carpinteria, CA; 1:100 in antibody dilution buffer containing 1% BSA, 0.1% cold fish skin gelatin, 0.5% Triton X-100, 0.05% sodium azide and 0.01 M PBS, pH 7.4). Following three 5-minute rinses in PBS containing 0.05% TWEEN-20, flat mounts were incubated for 45 min with Alexa fluor 488 (AF488) conjugated secondary antibody diluted 1:100 in PBST. Coverslips were placed over flat mounts together with Antifade™ medium. All reagents were purchased from Invitrogen (Carlsbad, CA) unless otherwise specified. Fluorescent images were collected as TIFF images at 1024 × 1024-pixel of resolution and 8-bits of depth with a confocal microscope (FluoView FV1000, Olympus, Center Valley, PA). Six lesions were identified around the macular using a 4× objective lens and the images of vascular structure were recorded.

2.8. CNV area scoring

Histological analysis of CNV lesions was performed using previously described methods (Kwak et al., 2000; Lai et al., 2001; Yanagi et al., 2002; Takahashi et al., 2006). Briefly, images were collected from serial sections spanning the entire length of each lesion with a microscope (Nikon Eclipse 80i) at ×100 magnification attached to a Micropublisher RTV 3.3 digital camera. Only lesions with clearly defined and good quality sections throughout the entire lesion were analyzed by this approach. Approximately 30 sections were examined for each lesion, with the observer masked to treatment. Images were imported into ImageJ (NIH) and the freehand selection tool used to delineate the boundaries of CNV complexes and the total area of each lesion across all sections was measured and expressed in square micrometers (μm^2) to determine maximum CNV complex area.

2.9. Statistical analyses

Graded lesion scoring was analyzed using the Fisher's exact probability test. Relative fluorescein intensities, determined by ImageJ analysis, were logarithmically transformed prior to one-way ANOVA analysis. Data are expressed as means ± SEM. In those cases in which data were logarithmically transformed, geometric means ± SE estimated using the Taylor series expansion are shown. The Tukey–Kramer method was applied for multiple comparisons.

Effect of bevacizumab on fluorescein intensity and histopathology were compared with vehicle-treated controls by performing a *t*-test on raw data. Statistics were performed using JMP (SAS Institute, Cary, NC) with P values < 0.05 considered statistically significant.

3. Results

The studies described here were designed to both optimize laser parameters (initial study) and validate this model of laser-induced CNV for use in screening novel therapeutics (bevacizumab efficacy study). Critical to the exploration of optimal laser power parameters is assessing both the incidence of neovascularization and the incidence of adverse effects that might necessitate procedural modifications or additional study design considerations. Hemorrhaging may occur as a result of laser-induced disruption of Bruch's membrane, potentially confounding disease modeling. In African green monkeys laser-induced hemorrhaging was observed at laser powers of 550 mW and above (Table 1). Minor hemorrhaging was observed in one or two spots in several eyes and fully resolved within 28 days. Severe hemorrhaging was less common, restricted to eyes receiving 750 mW or higher and did not fully resolve within 4 weeks, resulting in some exclusion of eyes from the analysis (Table 1).

Grade IV CNV, hallmarked by early and mid-transit hyperfluorescence and late phase fluorescein leakage beyond lesion borders (Fig. 1), was observed at 550–1500 mW power (Table 2). At the lowest laser power assessed, 350 mW, no grade IV lesions were observed (Fig. 1, Table 2). Application of 950 mW laser power resulted in significantly higher incidence of grade IV lesions at week 4 ($P = 0.0465$; 950 *vs* 550 mW; Fig. 1) with overall incidence of 19.4% in the treated eyes (Table 2, Fig. 2A). Separate experiments using the same laser spot size and duration settings were conducted to evaluate the effects of 1500 mW laser power on grade IV lesion incidence. Use of 1500 mW laser power yielded a higher incidence of grade IV lesions than 950 mW and resulted in similar incidence of hemorrhaging (Tables 1 and 2).

Table 1
Impact of laser power on incidence of hemorrhage.

Animal ID	Treatment (mW)	Presence of hemorrhage as result of laser treatment and status at week 4	
		Immediately post-laser	Week 4 post-laser
Y462	350	None	–
Y519	350	None	–
Y659	350	None	–
Y572	550	Minor, OS	Resolved
Y855	550	Minor, OS	Resolved
Y961	550	Minor, OS	Resolved
Y489	750	None	–
Y538	750	Minor, OS	Resolved
Y939	750	None	–
Y942	750	Minor, OD; severe, OS	Scarring, OS
Y539	950	Minor, OS	Resolved
Y586	950	Minor, OD; severe, OS	Sacrificed at day 22
Y598	950	Minor, OS	Resolved
Y727	950	None	–
Y887	1500	Minor, OD	Resolved
Y888	1500	Severe, OD	Scarring OD, excluded
Y924	1500	None	–
X477	1500	None	–

Retinal, subretinal and vitreal hemorrhaging was classified as minor or severe immediately post-laser. Resolved indicates absence of any retinal scarring that might adversely impact fluorescein angiography results. Scarring indicates one or more laser-induced lesions not fully resolved at week 4 and potentially requiring exclusion of this eye from analysis. Y586 was sacrificed at week 3 to evaluate pathology in a severely hemorrhaged eye.

Assessment of CNV development time course from 3 to 5 weeks post-laser treatment revealed that peak incidence of grade IV lesions occurred by week 4 in the 550–950 mW treatment groups (Fig. 2A). There was no significant difference in the incidence of grade IV lesions from week 3 to week 4 or week 4 to week 5 in any of these treatment groups. However, combined assessment of total grade III and IV lesions over the post-laser monitoring period demonstrated a significant increase in incidence from week 3 to week 4 at both 350 ($P < 0.0001$) and 750 mW ($P = 0.031$) laser power settings (Table 3). In parallel to graded scoring, fluorescein signal intensity in laser-induced lesions in late phase (6 min) angiograms was also determined (Fig. 2B). Background-corrected mean fluorescein intensity was determined across weeks 3–5 post-laser treatment. Peak fluorescein signal was observed at 4 weeks post-laser treatment in animals receiving 550, 750 or 950 mW. Overall peak signal intensity was observed in the 950 mW group. Application of higher laser power (1500 mW) resulted in further increases in peak fluorescein signal at 3–4 weeks post-laser (Fig. 2B).

An important consideration in establishing appropriate study group sizes for efficacy evaluations is not only overall incidence of CNV across all laser photocoagulation sites but also inter-eye variability in response. This is an issue rarely addressed in the literature but potentially critical to reliability of efficacy assessment. With respect to the incidence of grade III and grade IV lesion induction, we observed consistent grade III induction at 4 weeks post-laser with 750 mW or higher (Table 4). Grade IV lesions were observed in 25%, 33% and 71% of eyes in the 750, 950 and 1500 mW treatment groups, respectively. Late leakage, corresponding to lesions of grades III and IV, was accompanied by formation of neovascular vessels and development of CNV complex (Fig. 3), as demonstrated with both flat mounts (Fig. 3A, B) and classical H&E histological methodologies (Fig. 3C).

Final validation of the African green monkey laser-induced CNV model required demonstration of efficacy using an existing wet AMD therapeutic. Bevacizumab was administered intravitreally one day prior to laser treatment using 1500 mW laser power. Laser power of 1500 mW was selected for efficacy assessments to maximize grade IV CNV induction in the absence of therapeutic intervention. In vehicle-treated animals, there was extensive grade IV CNV induction and high fluorescein intensity within lesions (Fig. 4). Late phase hyperfluorescence, which extended beyond the lesion margins, was demonstrated in 3 out of the 6 lesions in the eye shown in Fig. 4 (upper panels). Evaluation of grade IV lesion incidence (Fig. 5A) revealed that bevacizumab treatment significantly blocked CNV as demonstrated by complete absence of grade IV lesions in the treated group (0% for bevacizumab vs. 31% for vehicle-treated animals; $P < 0.0001$). Bevacizumab-treated animals showed significantly lower late phase fluorescein intensity at 4 weeks post-laser compared to vehicle-treated controls (Fig. 5B, $P < 0.0001$). Quantitative histological examination of sections of the macular and perimacular region revealed significantly lower CNV area in bevacizumab-treated eyes compared to vehicle-treated animals ($P = 0.038$; Fig. 5C).

4. Discussion

This report provides the first published evaluation of laser-induced CNV methods in the African green monkey, a more accessible and equally predictive ophthalmic model than the rhesus and cynomolgus monkey. The wide use of African green monkeys in experimental research (Carlsson et al., 2004) and specific use in ophthalmic studies over several decades (Barany, 1963, 1977; Merrill and Burge, 2007) highlights their broad

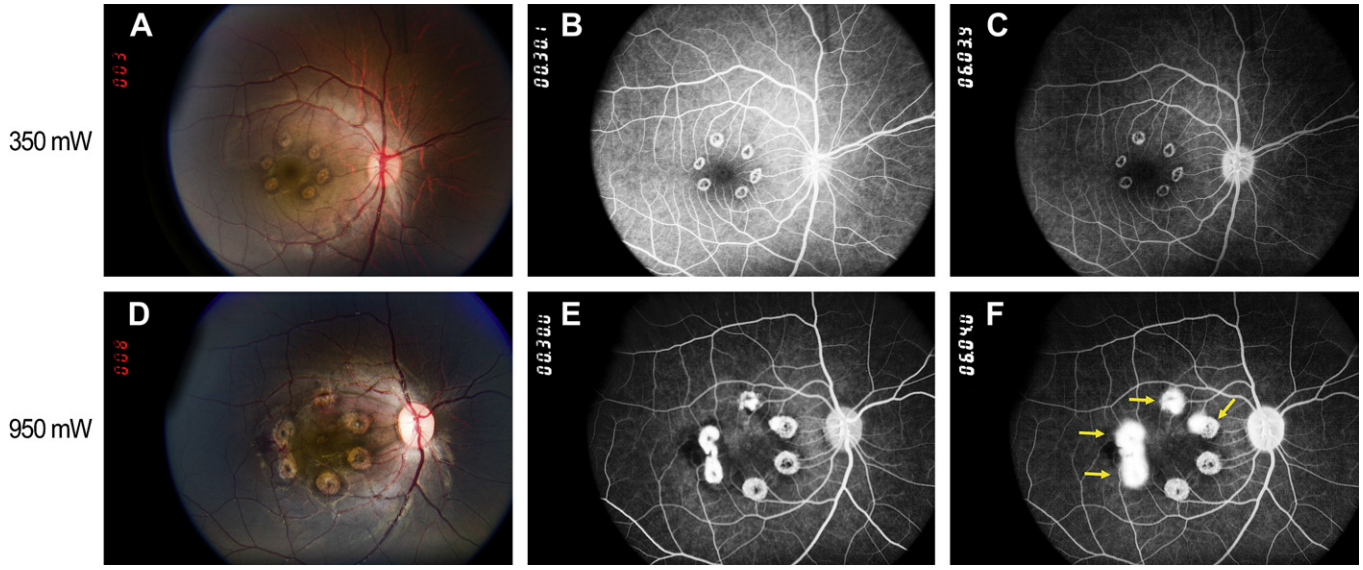

Fig. 1. Laser-induced hyperfluorescence and late leakage beyond borders. Fluorescein angiography of laser-induced CNV in monkeys following exposure to 350 mW (A–C) or 950 mW laser power (D–F). A and D represent color fundus images, B, E and C, F represent early phase (30 s) and late phase (6 min) angiograms respectively. 350 mW laser power did not induce grade IV CNV lesions (A–C, animal Y659). In eyes receiving 950 mW laser power extensive late leakage beyond borders (defined as grade IV lesions, yellow arrows) was observed (F, animal Y539).

preclinical model validity, availability and suitability for preclinical CNV modeling.

We observed laser-induced CNV in eyes within 3–4 weeks of laser treatment similar to previous reports in other nonhuman primates (Miller et al., 1995; Shen et al., 2002; Zhang et al., 2008). Incidence of grade IV CNV lesions increased with laser power and at 950 mW and 1500 mW powers 19.4% and 31.0% grade IV lesion incidence was observed respectively, corresponding with an earlier report (Krzystolik et al., 2002). Other reports have detailed slightly higher incidence of grade IV CNV in similar nonhuman primate models (Zhang et al., 2008; Lichtlen et al., 2010) although it is unclear how many of such grade IV lesions are a result of multiple hits at or immediately proximal to the initial laser photocoagulation site. Importantly, by week 4 even at the lowest laser powers employed in the present study, all laser-induced lesions were scored at grade II or above by masked examiners. A recent report, together with our own observations, indicate that grade III lesions and to a lesser extent, grade II lesions (Lichtlen et al., 2010) are also pathologically significant in that they can elicit neovascularization.

Table 2
Effect of laser power on incidence of CNV.

Treatment	Number of lesions (% of total lesions) at 4 weeks post-laser				Total number of lesions
	Grade I	Grade II	Grade III	Grade IV	
350 mW	0 (0)	20 (55.6)	16 (44.4)	0 (0)	36
550 mW	0 (0)	22 (61.1)	13 (36.1)	1 (2.8)	36
750 mW	0 (0)	11 (22.9)	35 (72.9)	2 (4.2)	48
950 mW	0 (0)	4 (11.1)	25 (69.4)	7 (19.4)*	36
1500 mW	0 (0)	13 (31.0)	16 (38.1)	13 (31.0)	42

Incidence of grade IV lesions was evaluated using Fisher's exact probability test and significantly higher incidence (denoted by *) was observed in eyes receiving 950 mW laser power compared to 350 mW ($P = 0.0102$) and 550 mW ($P = 0.0465$) laser treatment. Data was also analyzed when combining grade III and grade IV incidence based upon demonstration of histopathologic CNV in grade III lesions. Both 750 mW ($P = 0.0022$ vs. 350 mW and $P = 0.0004$ vs. 550 mW) and 950 mW ($P < 0.0001$ vs. 350 mW and $P < 0.0001$ vs. 550 mW) laser power induced significantly higher incidence of CNV when defined as grade III or IV. Assessment of 1500 mW laser power effects was performed in separate experiments and was not included in statistical analyses.

At 950 mW laser power, we observed grade III or IV CNV in close to 90% of all lesions, highlighting the importance of considering pathological outcome alongside classical graded angiography scoring when defining a new and clinically relevant experimental model. A number of reports have defined clinically relevant laser-induced CNV by grouping incidence data of both grade III and IV lesions and there is certainly merit to this approach based on the associated pathology; nonetheless, in accurately defining therapeutic benefits across multiple potential disease mechanisms it is critical to utilize the full dynamic range of the analytical methods employed, as highlighted recently by Lichtlen and co-workers (Lichtlen et al., 2010).

Although widely used and well-accepted in preclinical modeling, graded scoring of fluorescein angiograms still requires somewhat subjective assessment by examiners. As a graded scoring regimen, statistical methods available for discrimination of effects between ordinal values are more limited and certainly less powerful than for continuous values. As a result, reductions in CNV severity following therapeutic delivery may fail to show significance by graded angiographic criteria when histopathological or other angiography-based continuous value assessments do suggest significant improvement, thus complicating the process of efficacy determination. Furthermore, the lack of dynamic range inherent to the graded scoring method greatly limits any use of intra-eye assessments over a multi-time point study. Based on these notable limitations, we evaluated the use of a more quantitative and potentially high-throughput scoring strategy to define intensity of fluorescein signal within laser spots at multiple intervals post-laser treatment similar to methods described previously (Takahashi et al., 2006; Lichtlen et al., 2010). Observations from these assessments corroborated findings from graded scoring, but more importantly served to highlight the potential use of this analytical approach to studies evaluating efficacy over a course of fluorescein angiography sessions spanning weeks or months.

Another critical factor in defining appropriate laser power for laser-induced CNV modeling is the incidence of retinal, subretinal or vitreal hemorrhaging. There are very few reports detailing hemorrhaging as a result of experimental laser-induced CNV, and when described, is generally only referred to anecdotally (Shen

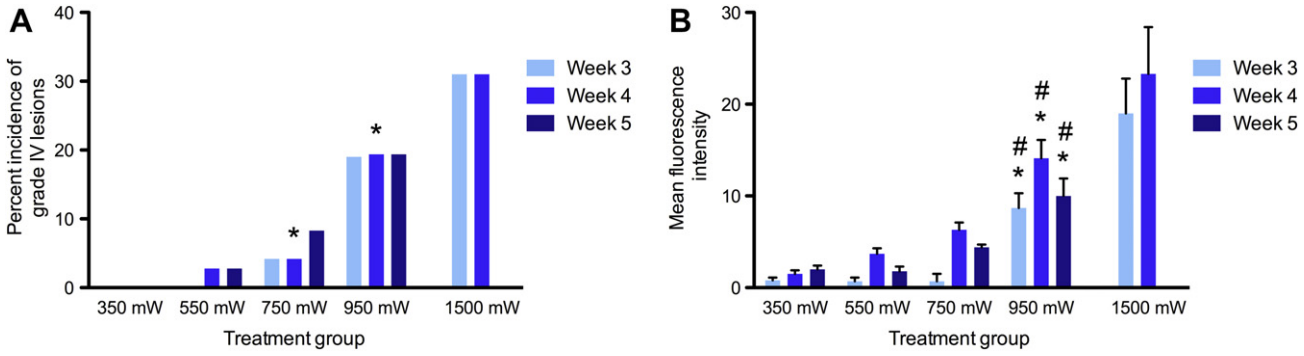

Fig. 2. Effect of Laser Power on CNV Development. Angiograms were scored by masked examiners at 3–5 weeks post-laser treatment using an I–IV grading system or ImageJ analysis of fluorescein intensity. Incidence of grade IV lesions increased with laser power (A) but only modestly increased beyond week 3. Background-corrected lesion fluorescein intensity also increased with laser power but demonstrated peak signal at 4 weeks post-laser (B). Data are presented as means and vertical bars indicate S.E.M. ($n = 30–48$). Symbols denote $P < 0.05$ compared to equivalent time point post-laser with 550/350 mW (*) or 750 mW (#) power (analysis performed on 4 week angiography results using Fisher's exact probability test). 1500 mW data was analyzed separately therefore no statistical analyses were performed to compare 350–950 mW laser power with 1500 mW laser power results.

et al., 2004; Koh et al., 2006). However, this is a critical consideration when defining optimal laser parameters and acceptable attrition for animal or eye exclusion within a study. In the present study, incidence of hemorrhaging was confined to laser power of 750 mW and higher, but never resulted in exclusion of more than one eye per treatment group. Our observations, together with the limited reports in the literature suggest that when defining group sizes for a preclinical evaluation one must always consider the inherent possibility of hemorrhaging and account for possible exclusions from treatment group in the study design.

Histopathological assessment of laser-induced CNV historically has relied on either area assessments of CNV complex across serial transverse sections of the laser lesion (Yanagi et al., 2002) or area assessments from choroidal flat mounts collected after administration of FITC-dextran or fluorescein-labeled tomato lectin (Campa et al., 2008). We found these endpoints to be complementary in our model validation, with advantages to both. Classical histology sections enable more thorough assessment of the CNV complex, while flat mounts are quicker to produce and provide a more direct correlate with fluorescein angiograms.

To validate the African green monkey laser-induced CNV model we examined the efficacy of intravitreally administered bevacizumab compared to vehicle-treated controls. Our findings demonstrated complete inhibition of laser-induced grade IV CNV by bevacizumab treatment. In addition, fluorescein intensity assessments similarly illustrated significant attenuation of fluorescein signal in laser spots, supporting a recent and thus far only other report of bevacizumab efficacy in nonhuman primates (Lichtlen et al., 2010). Despite similar efficacy in both models important differences exist between this prior study and our findings, including species selection, laser parameters, dosing regimen and analytical methods. In the present study a single IVT dose of bevacizumab, administered 1 day prior to laser treatment demonstrated similar efficacy to a 3-dose regimen employed in the prior report (Lichtlen et al., 2010). These findings highlight the importance of evaluating mechanism of action during the study design process to enable use of minimal dosing to achieve maximal efficacy. VEGF expression induced as a result of laser-induced disruption of Bruch's membrane reportedly peaks in the RPE/choroid between days 3 and 7 post-laser (Hu et al., 2009) and these findings provided the basis for timing of bevacizumab dosing in the present study. An additional dose regimen consideration included the inherent risk of endophthalmitis with any IVT injection. In both the clinical and preclinical setting, the therapeutic goal must be to minimize dosing intervals when utilizing this delivery approach.

In summary, African green monkeys offer the same benefits in preclinical modeling of wet AMD using a laser-induced CNV approach offered by other Old World primates such as cynomolgus and rhesus monkeys, while offering the advantage of wider availability and potentially lower cost. Our studies also highlight

Table 3
Time course of CNV development following laser treatment.

Treatment	Study week	No. lesions analyzed	Incidence (% incidence)			
			Grade I	Grade II	Grade III	Grade IV
350 mW	3	30	0 (0)	30 (100)	0 (0)	0 (0)
	4	36	0 (0)	20 (56)	16 (44)	0 (0)
	5	36	0 (0)	18 (50)	18 (50)	0 (0)
550 mW	3	36	0 (0)	23 (64)	13 (36)	0 (0)
	4	36	0 (0)	22 (61)	13 (36)	1 (3)
	5	36	0 (0)	21 (58)	14 (39)	1 (3)
750 mW	3	48	1 (2)	21 (44)	23 (48)	3 (6)
	4	48	0 (0)	11 (23)	35 (73)	2 (4)
	5	48	0 (0)	5 (10)	39 (81)	4 (8)
950 mW	3	42	0 (0)	4 (10)	30 (71)	8 (19)
	4	36	0 (0)	4 (11)	25 (69)	7 (19)
	5	36	0 (0)	4 (11)	25 (69)	7 (19)
1500 mW	3	42	0 (0)	16 (38)	13 (31)	13 (31)
	4	42	0 (0)	13 (31)	16 (38)	13 (31)

In the 350 mW treatment group, a single eye was excluded from week 3 analysis due to blurring of late phase angiogram. In the 950 mW treatment group animal Y586 was sacrificed upon completion of week 3 angiogram collection due to hemorrhaging in left eye and to enable evaluation of hemorrhage pathology. Analysis of animals receiving 1500 mW laser power was only performed on weeks 3 and 4 post-laser. Significant increases in incidence of grade III and IV lesions were observed between week 3 and week 4 at 350 ($P < 0.0001$) and 750 mW ($P = 0.031$) laser power.

Table 4
Assessment of inter-eye variability in CNV induction following laser treatment.

Treatment group	Incidence of grade III or IV lesions (%)	Incidence of grade IV lesions (%)
350 mW	4/6 (67%)	0/6 (0%)
550 mW	5/6 (83%)	1/6 (17%)
750 mW	8/8 (100%)	2/8 (25%)
950 mW	6/6 (100%)	2/6 (33%)
1500 mW	7/7 (100%)	5/7 (71%)

Values represent number (and percent) of eyes with one or more grade III or grade IV lesions at 4 weeks post-laser treatment.

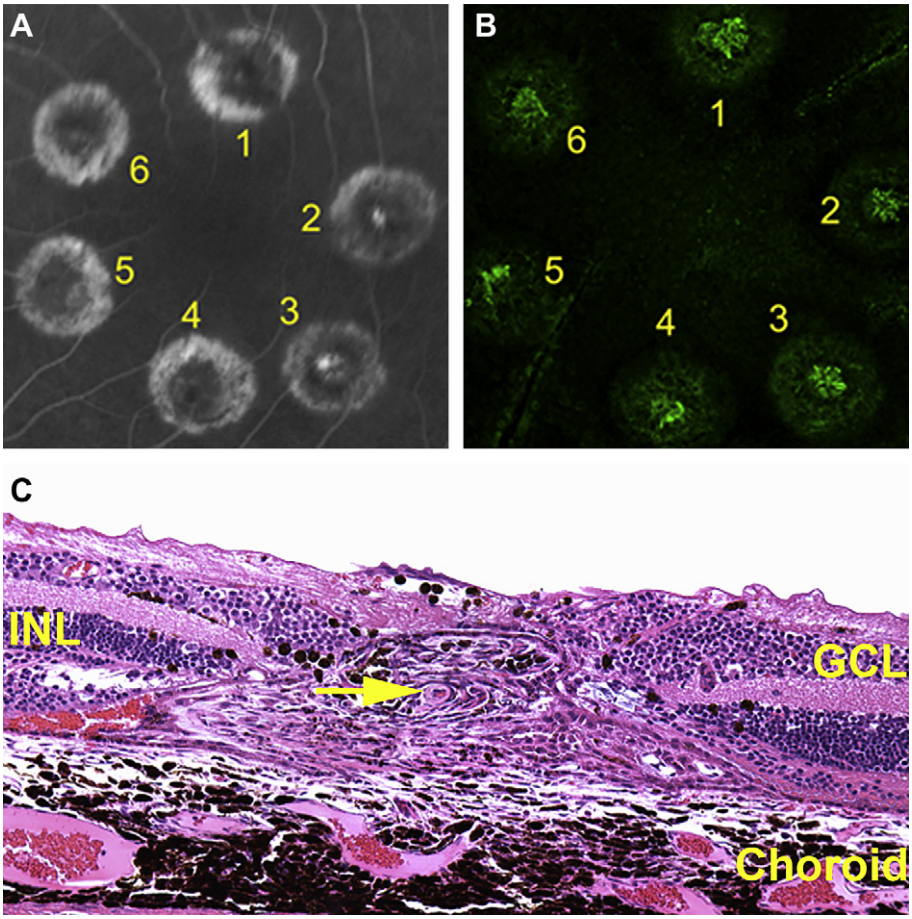

Fig. 3. Laser-induced choroidal neovascularization. Fluorescein angiogram illustrates late phase hyperfluorescence and leakage (A). Lesions for illustrated eye (animal Y598 OS) were scored as follows: lesion 1 = grade III; lesion 2 = grade III; lesion 3 = grade II; lesion 4 = grade III; lesion 5 = grade III; lesion 6 = grade III. Anti-von Willebrand Factor (anti-vWF) staining highlights neovascular vessels (B) and transverse section of laser-induced lesion demonstrates CNV formation and neovascular vessel (C). Abbreviations: GCL = ganglion cell layer; IPL = inner plexiform layer. Arrow identifies neovascular vessel.

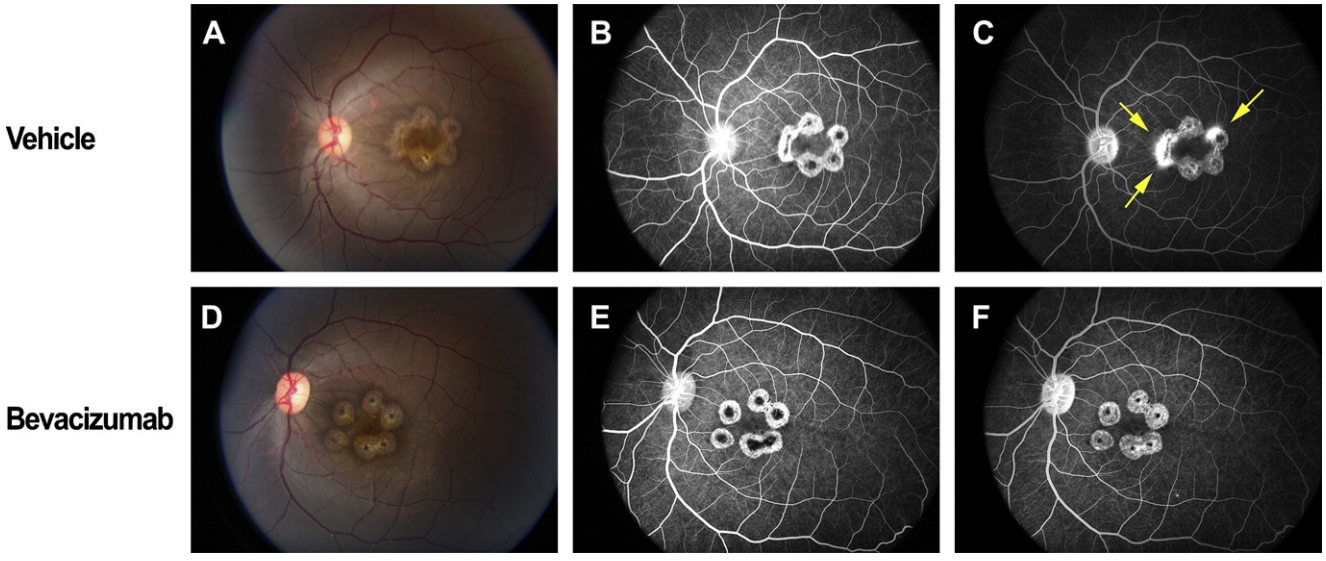

Fig. 4. Bevacizumab attenuates laser-induced CNV. Fluorescein angiography of vehicle and bevacizumab (IVT delivery of 1.25 mg/eye, 1 day prior to laser photocoagulation) treated eyes at 4 weeks post photocoagulation. Images provide representative examples of color fundus (A, D), early phase (30 s; B, E) and late phase (6 min; C, F) angiograms. In vehicle-treated eyes hyperfluorescence and late leakage beyond borders was observed (grade IV lesions identified by arrows in panel C), whereas bevacizumab-treated eyes demonstrate no late leakage beyond borders (panel F). In illustrated representative vehicle-treated eye graded scoring was as follows: lesion 1 (12 o'clock position, all subsequent lesions graded clockwise) = grade II; lesion 2 = grade IV; lesion 3 = grade II; lesion 4 = grade III; lesion 5 = grade IV; lesion 6 = grade IV. For representative bevacizumab-treated eye, scoring was as follows: lesion 1 = grade II; lesion 2 = grade II; lesion 3 = grade III; lesion 4 = grade III; lesion 5 = grade III; lesion 6 = grade II.

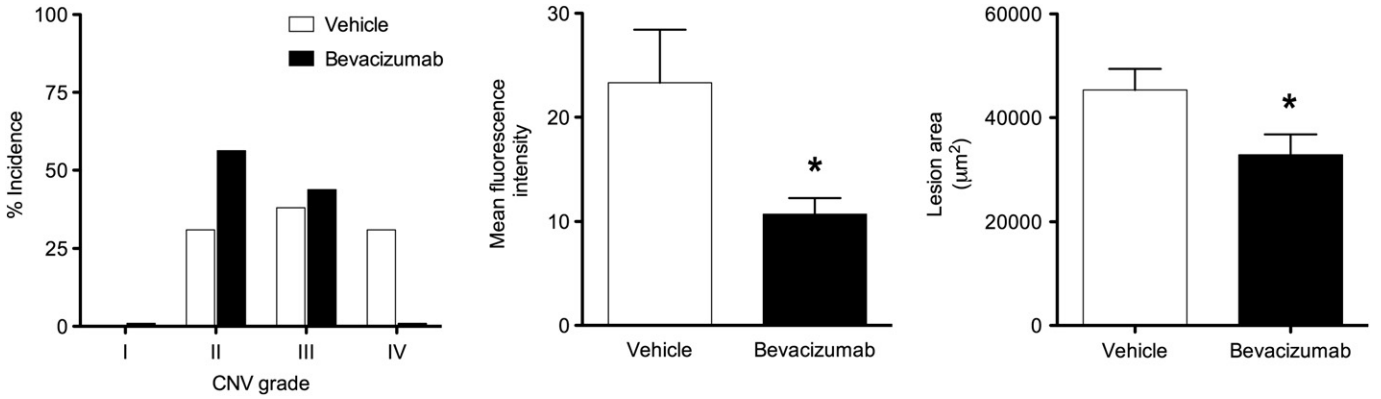

Fig. 5. CNV leakage and area is reduced by bevacizumab. Laser treatment (1500 mW) induced grade IV lesions in vehicle-treated eyes but no grade IV lesions were observed in eyes receiving bevacizumab (A; $P < 0.0001$). Fluorescein intensity was also significantly lower ($P < 0.0001$) within lesions of bevacizumab-treated eyes compared to vehicle-treated controls (B). Bevacizumab significantly attenuated CNV area development (C) compared with vehicle-treated controls ($P = 0.038$). Data shows absolute percent incidence (A), mean fluorescence intensity values (B) or mean maximum CNV area in μm^2 with vertical bars indicating SEM (7–8 eyes analyzed per group).

important methodological considerations that should not be overlooked when evaluating therapeutic candidates for treatment of wet AMD, regardless of test species used.

Conflict of interest

WH, AS, SB, FJL were employees at Bausch & Lomb during the experimental analysis described in this manuscript. Bausch & Lomb develops and manufactures ophthalmic drugs and devices and provide financial support towards components of detailed model development.

Acknowledgements

The authors would especially like to thank Karen Condello for logistical support and both Steve Henry and Rohn Brookes for technical assistance in animal studies.

References

Barany, E., 1963. Applanation tonometry and ophthalmoscopy of the vervet monkey (*Cercopithecus aethiops*) in phencyclidine catalepsia. Invest. Ophthalmol. 2, 322–324.

Barany, E.H., 1977. Pilocarpine-induced subsensitivity to carbachol and pilocarpine of ciliary muscle in vervet and cynomolgus monkeys. Acta Ophthalmol. (Copenh) 55, 141–163.

Campa, C., Kasman, I., Ye, W., Lee, W.P., Fuh, G., Ferrara, N., 2008. Effects of an anti-VEGF-A monoclonal antibody on laser-induced choroidal neovascularization in mice: optimizing methods to quantify vascular changes. Invest. Ophthalmol. Vis. Sci. 49, 1178–1183.

Carlsson, H.E., Schapiro, S.J., Farah, I., Hau, J., 2004. Use of primates in research: a global overview. Am. J. Primatol. 63, 225–237.

Ciulla, T.A., Rosenfeld, P.J., 2009. Antivascular endothelial growth factor therapy for neovascular age-related macular degeneration. Curr. Opin. Ophthalmol. 20, 158–165.

Francois, J., De Laey, J.J., Cambie, E., Hanssens, M., Victoria-Troncoso, V., 1975. Neovascularization after argon laser photocoagulation of macular lesions. Am. J. Ophthalmol. 79, 206–210.

Green, W.R., 1999. Histopathology of age-related macular degeneration. Mol. Vis. 5, 27.

Hu, W., Criswell, M.H., Fong, S.L., Temm, C.J., Rajashekhar, G., Cornell, T.L., Clauss, M.A., 2009. Differences in the temporal expression of regulatory growth factors during choroidal neovascular development. Exp. Eye Res. 88, 79–91.

Husain, D., Kim, I., Gauthier, D., Lane, A.M., Tsilimbaris, M.K., Ezra, E., Connolly, E.J., Michaud, N., Gragoudas, E.S., O'Neill, C.A., Beyer, J.C., Miller, J.W., 2005. Safety and efficacy of intravitreal injection of ranibizumab in combination with verteporfin PDT on experimental choroidal neovascularization in the monkey. Arch. Ophthalmol. 123, 509–516.

Kim, I.K., Husain, D., Michaud, N., Connolly, E., Lane, A.M., Durrani, K., Hafezi-Moghadam, A., Gragoudas, E.S., O'Neill, C.A., Beyer, J.C., Miller, J.W., 2006. Effect of intravitreal injection of ranibizumab in combination with verteporfin PDT on normal primate retina and choroid. Invest. Ophthalmol. Vis. Sci. 47, 357–363.

Koh, H.J., Freeman, W.R., Azen, S.P., Flaxel, C.J., Labree, L.D., Cheng, L., Wills, M., Jones, T.R., 2006. Effect of a novel octapeptide urokinase fragment, A6, on experimental choroidal neovascularization in the monkey. Retina 26, 202–209.

Krzystolik, M.G., Afshari, M.A., Adamis, A.P., Gaudreault, J., Gragoudas, E.S., Michaud, N.A., Li, W., Connolly, E., O'Neill, C.A., Miller, J.W., 2002. Prevention of experimental choroidal neovascularization with intravitreal anti-vascular endothelial growth factor antibody fragment. Arch. Ophthalmol. 120, 338–346.

Kwak, N., Okamoto, N., Wood, J.M., Campochiaro, P.A., 2000. VEGF is major stimulator in model of choroidal neovascularization. Invest. Ophthalmol. Vis. Sci. 41, 3158–3164.

Lai, C.C., Wu, W.C., Chen, S.L., Xiao, X., Tsai, T.C., Huan, S.J., Chen, T.L., Tsai, R.J., Tsao, Y.P., 2001. Suppression of choroidal neovascularization by adeno-associated virus vector expressing angiostatin. Invest. Ophthalmol. Vis. Sci. 42, 2401–2407.

Lichtlen, P.D., Lam, T., Nork, M., Streit, T., Urech, D.M., 2010. Relative contribution of VEGF and TNF-alpha in the cynomolgus laser-induced CNV model: comparing efficacy of bevacizumab, adalimumab and ESBA105. Invest. Ophthalmol. Vis. Sci. 51, 4738–4745.

Lu, F., Adelman, R.A., 2009. Are intravitreal bevacizumab and ranibizumab effective in a rat model of choroidal neovascularization? Graefes Arch. Clin. Exp. Ophthalmol. 247, 171–177.

Marano, R.J., Rakoczy, P.E., 2006. An improved method using densitometry for evaluating severity of laser photocoagulation induced CNV. Biotech. Histochem. 81, 59–62.

Marano, R.J., Toth, I., Wimmer, N., Brankov, M., Rakoczy, P.E., 2005. Dendrimer delivery of an anti-VEGF oligonucleotide into the eye: a long-term study into inhibition of laser-induced CNV, distribution, uptake and toxicity. Gene Ther. 12, 1544–1550.

Merrill, N.L., Burge, R., 2007. Effects of three mydriatic drug regimens on pupil size in rhesus (*Macaca mulatta*) and African green monkeys (*Chlorocebus aethiops*). J. Med. Primatol. 36, 33–38.

Miller, J.W., Walsh, A.W., Kramer, M., Hasan, T., Michaud, N., Flotte, T.J., Haimovici, R., Gragoudas, E.S., 1995. Photodynamic therapy of experimental choroidal neovascularization using lipoprotein-delivered benzoporphyrin. Arch. Ophthalmol. 113, 810–818.

Ozkiris, A., 2010. Anti-VEGF agents for age-related macular degeneration. Expert Opin. Ther. Pat. 20, 103–118.

Resnikoff, S., Pascolini, D., Etya'ale, D., Kocur, I., Pararajasegaram, R., Pokharel, G.P., Mariotti, S.P., 2004. Global data on visual impairment in the year 2002. Bull. World Health Organ. 82, 844–851.

Rosenfeld, P.J., Brown, D.M., Heier, J.S., Boyer, D.S., Kaiser, P.K., Chung, C.Y., Kim, R.Y., 2006. Ranibizumab for neovascular age-related macular degeneration. N. Engl. J. Med. 355, 1419–1431.

Ryan, S.J., 1979. The development of an experimental model of subretinal neovascularization in disciform macular degeneration. Trans. Am. Ophthalmol. Soc. 77, 707–745.

Ryan, S.J., 1982. Subretinal neovascularization. Natural history of an experimental model. Arch. Ophthalmol. 100, 1804–1809.

Shen, W.Y., Garrett, K.L., Wang, C.G., Zhang, K., Ma, Z.Z., Constable, I.J., Rakoczy, P.E., 2002. Preclinical evaluation of a phosphorothioate oligonucleotide in the retina of rhesus monkey. Lab. Invest. 82, 167–182.

Shen, W.Y., Lee, S.Y., Yeo, I., Lai, C.M., Mathur, R., Tan, D., Constable, I.J., Rakoczy, P.E., 2004. Predilection of the macular region to high incidence of choroidal neovascularization after intense laser photocoagulation in the monkey. Arch. Ophthalmol. 122, 353–360.

Takahashi, H., Obata, R., Tamaki, Y., 2006. A novel vascular endothelial growth factor receptor 2 inhibitor, SU11248, suppresses choroidal neovascularization in vivo. J. Ocul. Pharmacol. Ther. 22, 213–218.

Tolentino, M.J., Husain, D., Theodosiadis, P., Gragoudas, E.S., Connolly, E., Kahn, J., Cleland, J., Adamis, A.P., Cuthbertson, A., Miller, J.W., 2000. Angiography

of fluoresceinated anti-vascular endothelial growth factor antibody and dextrans in experimental choroidal neovascularization. Arch. Ophthalmol. 118, 78–84.
Yanagi, Y., Tamaki, Y., Obata, R., Muranaka, K., Homma, N., Matsuoka, H., Mano, H., 2002. Subconjunctival administration of bucillamine suppresses choroidal neovascularization in rat. Invest. Ophthalmol. Vis. Sci. 43, 3495–3499.
Yu, L., Wu, X., Cheng, Z., Lee, C.V., LeCouter, J., Campa, C., Fuh, G., Lowman, H., Ferrara, N., 2008. Interaction between bevacizumab and murine VEGF-A: a reassessment. Invest. Ophthalmol. Vis. Sci. 49, 522–527.
Zhang, M., Yan, M., Wang, L., Zhang, J.J., Liu, B., Meng, D., Du, C.F., 2008. Experimental choroidal neovascularization induced by laser in the eyes of rhesus monkeys. Sichuan Da Xue Xue Bao Yi Xue Ban 39, pp. 567–569, 574.